Chapter 6

Photocatalytic Hydrogen Production with Visible Light over Pt-Interlinked Hybrid Composites of Cubic-Phase and Hexagonal-Phase CdS

Sections reprinted with permission from Silva, L.A.; Ryu, S.Y.; Choi, J.; Choi, W.; Hoffmann, M. R. *Journal of Physical Chemistry C* **2008**, *112*, 12069.

Abstract

A hybrid photocatalytic system, which is based on a mixed-phase cadmium sulfide matrix composed of nano-particulate cubic-phase CdS (c-CdS) with average particle diameters of 13 nm and a bandgap energy of 2.6 eV, is coupled with bulk-phase hexagonal CdS (hex-CdS) that has a bandgap energy of 2.3 eV and is interlinked with elemental platinum deposits. The resulting hybrid nano-composite catalysts are photocatalytically efficient with respect to hydrogen gas production from water with visible light irradiation at $\lambda > 420$ nm. Rates of H_2 production approaching 1.0 mmol-H_2 g^{-1} h^{-1} are obtained with a c-CdS/Pt/hex-CdS composite photocatalyst, in the presence of a mixed sodium sulfide and sodium sulfite background electrolyte system at pH 14. In contrast, the same composite produces H_2 at a rate of 0.15 mmol g^{-1} h^{-1} at pH 7 in a water-isopropanol solvent system. The relative order of reactivity for the synthesized hybrid catalysts was found to be: c-CdS/Pt/hex-CdS > Pt/c-CdS/hex-CdS > c-CdS/hex-CdS > Pt/hex-CdS > hex-CdS > quantum-sized c-CdS. A mechanism involving enhanced lifetimes of electron-hole trapping states that are dependent on the surface chemistry of hydrated CdS involving surface hydroxyl (>CdOH) and sulfhydryl groups (>CdSH) are invoked.

Introduction

Photocatalytic splitting of water using metal oxide or metal sulfide semiconductors and sunlight may provide an alternative approach to convert water into hydrogen and oxygen. For example, bulk-phase cadmium sulfide in the cubic form, c-CdS, which has a nominal band gap energy of 2.4 eV and appropriate band positions, has the thermodynamic potential to drive water-splitting with visible light illumination[1-7].

$$2\,H_2O \xrightarrow[h\nu]{CdS} 2\,H_2 + O_2 \qquad (6.1)$$

Cubic-phase CdS (c-CdS) is readily obtained by sol-gel procedures using mixed aqueous solutions of an appropriate cadmium salt mixed with sodium sulfide at low temperatures. In contrast, the synthesis at high temperature results in the formation of hexagonal-phase CdS (hex-CdS) in a 'wurtzite' crystal structure. Matsumura et al.[2] reported that higher H_2 production rates and higher photo-efficiencies are obtained with bulk-phase hex-CdS when compared to bulk-phase c-CdS suspensions.

In the case of quantum-sized (Q-sized) c-CdS produced by sol-gel methods, the band edges are shift to yield larger overall redox potentials[8-10]. For example, Hoffman et al. prepared c-CdS in gylcerol with average particle diameters of 4 nm and band gap energies shifted to 3.1 eV[11]. The increased thermodynamic driving force of the 3.1 eV particles should increase the net rate of interfacial charge transfer in the normal Marcus regime[12-14], and thus result in higher rates and efficiencies of photocatalysis[15]. In this regard, Hoffman et al.[16] reported a tenfold increase in the photo-efficiency for production of H_2O_2 on quantum-sized ZnO as the particle diameters were decreased from 4.0 to 2.3 nm, while similar effects were observed during the photo-polymerization of methylmethacrylate (MMA), as initiated by CdS, ZnO, and TiO_2. In each case, the

photo-initiated polymerization of MMA on quantum-sized particles of CdS, ZnO, and TiO_2 resulted in much higher quantum yields and mass production rates, when compared to their bulk-phase counterparts at the same total surface area[11,17].

In an effort to increase the photo-activity of CdS with respect to hydrogen production from water in the presence of sacrificial electron donors, we have synthesized a series of hybrid catalytic systems that couple the higher efficiency hexagonal phase CdS (hex-CdS) in the bulk-phase size domain with quantum-sized cubic-phase CdS interlinked with elemental Pt deposits. The overall goal is to increase higher photoefficiencies for water splitting with hybrid catalytic systems.

Experimental

Bulk-phase, hex-CdS (orange crystallites) was synthesized by the thermal treatment (i.e., calcination) of commercial-grade c-CdS (Aldrich, yellow powders) at 800 ^{o}C under a flowing-nitrogen atmosphere for one hour. The nano-composite photocatalysts were prepared using several different procedures. In the first procedure, quantum-sized c-CdS was prepared *in situ* as a colloidal suspension in ethanol as described previously[11] and subsequently deposited directly on to the much larger hex-CdS crystallite surfaces. In a second synthetic step, metallic platinum was deposited on the hybrid c-CdS/hex-CdS aggregates by the photodecomposition of $PtCl_6^{2-}$ to form Pt/c-CdS/hex-CdS nanocomposite. In a separate procedure, elemental platinum was photodeposited on the hex-CdS surfaces before c-CdS deposition to form c-CdS/Pt/hex-CdS composite. c-CdS deposition on to 1.0 g of the base substrate [hex-CdS or Pt/hex-CdS] surface was accomplished by mixing 20 mL of a 0.01 M Cd^{2+} solution into ethanol with stirring for

one day at room temperature. After 24 hours, a stoichiometric amount of Na_2S was added to the Cd^{2+}/hex-CdS or Cd^{2+}/Pt/hex-CdS suspensions. The reaction products were filtered, washed with ethanol, and air dried.

The Pt-loaded hybrid particles were prepared by irradiation of hex-CdS or c-CdS/hex-CdS suspensions (1.0 g in 50 mL of a mixed solvent H_2O/isopropanol (70:30 v/v)) for 30 min using a 500-W xenon-arc lamp in the presence of $H_2PtCl_6 \cdot 6H_2O$ (0.3 wt% of Pt). The final pH of the solution after photodeposition was 4. After irradiation, the filtered Pt-loaded samples were washed with distilled water and ethanol. The resulting nanocomposite catalysts were characterized by XRD, diffuse reflectance spectroscopy, TEM, and XPS analysis.

UV-vis diffuse reflectance spectra were recorded on a Shimadzu UV-2101PC with an integrating sphere attachment (Shimadzu ISR-260), using Ba_2SO_4 powder as an internal reference. SEM images were taken on a LEO 1550VP FESEM while XRD spectra were recorded on a Phillips X-Pert PRO X-ray diffraction system. XPS measurements were made with an M-probe surface spectrometer (VG Instruments) using monochromatic Al K_α X-rays (1486.6 eV).

A high-pressure Hg-Xe arc lamp was used as the light source for the photolyses. The collimated light beam was passed through an IR filter, a focusing lens and a 400 nm cut-off filter before reaching the cyclindrical photolysis cell, which was air-cooled to maintain a constant temperature. Since it is well known that colloidal CdS suspensions undergo photocorrosion and photocatalytic dissolution under oxic conditions, H_2 production experiments were carried out under a nitrogen atmosphere. Before each

experiment, the quartz photolysis cell was purged with N_2 for 30 min in order to eliminate O_2.

Hydrogen gas evolution was measured using gas chromatography (HP 5890 Series II) with thermal conductivity detection (TCD). Due to similar conductivity values for He and H_2, nitrogen was used as a carrier gas. The separations were achieved with a molecular sieve column (30 m × 0.32 mm × 12.00 μm). The GC oven temperature was set at 30 ^{o}C in order to achieve the best spatial resolution between N_2 (i.e., the reactor purge gas) and H_2. Calibration curves were found to be linear over a broad range of H_2 concentrations.

In a typical photolysis experiment, 50 mg of a target hybrid photocatalyst preparation was dispersed 1) in an aqueous solution (total volume = 50 mL) containing 30% isopropanol or 2) in an aqueous solution (total volume = 50 mL) containing 0.1 M Na_2S, 0.02 M Na_2SO_3, and 1.0 M NaOH. The isopropanol and mixed sulfide (HS^-/S^{2-}; pK_{a2,H_2S} = 17.3) sulfite (HSO_3^-/SO_3^{2-} pK_{a2} = 7.2) were used as electron donors to prevent photo-corrosion of CdS. Sample aliquots of the headspace gas of the photolysis cell, where the total headspace volume was 100 mL, were taken with a gas-tight syringe in increments of 50 μL through a rubber septum. Multiple sample aliquots were taken at each time point to ensure precision.

Results and Discussion

The X-ray diffraction patterns of bulk-phase c-CdS and hex-CdS, which are shown in Figure 6.1, confirms that calcination of bulk-phase c-CdS at 800 ^{o}C results in the formation of hex-CdS in a highly-crystalline wurtzite structure. This result is consistent

with earlier reports[2,7]. On the other hand, the bulk-phase precursor, c-CdS, has an X-ray diffraction pattern that is typical of semi-amorphous materials.

The apparent bandgap energies for c-CdS and hex-CdS were determined from diffuse reflectance spectra as shown in Figure 6.2a. The corresponding bandgap energies, ΔE_g, were obtained: 1) 2.33 eV for bulk-phase c-CdS, 2) 2.31 eV for hex-CdS, and 3) 2.62 eV for nano-particulate c-CdS. The UV-vis spectrum of hex-CdS exhibits a sharp edge at 570 nm. In contrast, the corresponding spectrum of nano-particulate c-CdS is blue shifted by 0.3 eV compared to the corresponding bulk phase c-CdS or hex-CdS. The observed blue shift for Q-CdS is consistent with the much smaller sizes of the colloidal nano-particles compared to the micrometer-sized, bulk-phase c-CdS or hex-CdS powders[11].

For comparison, the diffuse reflectance spectra of the composite catalysts are shown in Figure 6.2b. The spectrum of the c-CdS/hex-CdS composite appears to be a linear combination of the individual spectra of the two CdS crystalline phases. The particle sizes of the base hex-CdS material range from 6–9 μm based on the TEM analysis. TEM micrographs of nano-particulate c-CdS clearly show Q-sized islands deposited on the surface of the Pt/hex-CdS core (i.e., c-CdS/Pt/hex-CdS) while, in constrast, the Pt/c-CdS/hex-CdS composite appears to be devoid of Q-sized islands. It appears that the specific sequence of photodeposition of Pt may control whether or not c-CdS remains attached to the core hex-CdS surface. Surface attached c-CdS islands are apparent only when the c-CdS is deposited during the last step in the composite catalyst preparation. The average particle diameter of c-CdS islands that were deposited on the hex-CdS surfaces is 13 nm.

Hydrogen generation rates were measured for the series of composite catalysts using either an aqueous solution of isopropanol at circum-neutral pH or an aqueous solution of a mixed sulfide (HS^-/S^{2-}) and sulfite (SO_3^{2-}) solution at high pH (pH 14), which was determined by the concentration of NaOH (1.0 M). The gaseous hydrogen production was measured during the first eight hours of irradiation at sampling intervals of two hours with the final sample aliquot taken after 22 hours of irradiation. In contrast, the dark control showed no H_2 production in the absence of light. In addition, suspensions of plain hex-CdS and Pt/hex-CdS were found to be photocatalytic with respect to H_2 production with time.

From the kinetic data shown in Table 6.1, it appears that the Pt/c-CdS/hex-CdS composite has very low catalytic activity with isopropanol as an electron donor, but it shows much higher activity at pH 14 with the mixed sulfide/sulfite electron donor system. In contrast, the c-CdS/Pt/hex-CdS hybrid composite yields much higher rates of H_2 production under the same irradiation conditions for both electron donor systems. When normalized to the weight of the catalyst sample, hydrogen production rates were found to be $d[H_2]/dt$ = 153 and 668 μmol g^{-1} h^{-1} for isopropanol (pH 7) as an electron donor and sulfide/sulfite as electron donors (pH 14), respectively. Nanoparticulate c-CdS islands on the Pt/hex-CdS surface have an average radius of 6.5 nm, while in contrast, on Pt/c-CdS/hex-CdS no c-CdS deposits were observed by TEM. In addition, XPS analysis shows that there is only one species of Cd (i.e., Cd(II)) present in c-CdS/Pt/hex-CdS composite, while the Pt/c-CdS/hex-CdS composite spectrum shows two different forms of cadmium. These results suggest that the c-CdS, which was deposited on the orange hex-CdS crystals, underwent photocorrosion during irradiation of $PtCl_6^{2-}$ to generate the

Pt(0) islands. Quantum-sized c-CdS is much less stable than bulk phase hex-CdS, due to its less crystalline structure and smaller particle size with a corresponding higher specific surface area-to-volume ratio.

In addition to the apparent loss of c-CdS due to photocorrosion, the lower activity of Pt/c-CdS/hex-CdS may be due to the presence of several higher oxidation state species of platinum on the surface. When a $4f_{7/2}$ peak is used as a reference, the binding energy of Pt(0) is determined to be 71.0 eV[4]. However, the XPS spectrum for Pt/c-CdS/hex-CdS has a $4f_{7/2}$ peak at 72.4 eV (not shown); the slight shift to higher energies indicates the presence of higher oxidation states of platinum. This observation is consistent with the results of Jin et al.[1] who reported that platinum sulfide, Pt(II)S, was formed instead of Pt(0) as the photo-reduction product of $PtCl_6^{2-}$ on bulk-phase c-CdS under acidic conditions in water. On the other hand, the XPS spectrum of c-CdS/Pt/hex-CdS sample has a binding energy of 71.6 eV close to Pt(0) reference peak of 71.0 eV.

The kinetic results tabulated in Table 6.1 indicate that Pt/c-CdS/hex-CdS has the highest hydrogen production rate in the sulfide/sulfite electron donor system that is substantially higher on a relative basis compared to isopropanol as the sole electron donor. In the case of the sulfide-sulfite electron-donor system, there appears to be no significant difference between rates of H_2 production from both Pt/c-CdS/hex-CdS and c-CdS/Pt/hex-CdS composites during the early stages of illumination. However, after 22 hours of continuous irradiation, the activity of the Pt/Q-CdS/hex-CdS composite was clearly lower. The average rates of hydrogen production for Pt/c-CdS/hex-CdS and c-CdS/Pt/hex-CdS composites were 537 $\mu mol\ g^{-1}h^{-1}$ and 668 $\mu mol\ g^{-1}h^{-1}$, respectively. In

the case of Pt/c-CdS/hex-CdS in the sulfide/sulfite electron system, SO_3^{2-} may substitute for S^{2-} which may have been lost from the surface lost during the photodeposition of platinum. In addition, during the course of irradiation, Pt(II) can be reduced back to Pt(0) at high pH; this may account for the increase in activity of Pt/c-CdS/hex-CdS at high pH compared to pH 7. The gradual change in the oxidation state of Pt during the course of photocatalytic reaction has been demonstrated previously in the case of Pt/TiO_2 catalysts[18]. Platinum oxides on TiO_2 are reduced to zero-valent platinum during irradiation.

The effect of quantum-sized c-CdS on hydrogen production rates can be seen in the data of Table 6.1. With isopropanol as the electron donor, the hydrogen production rate is increased 3.4-fold compared to samples without Q-sized c-CdS (c-CdS/Pt/hex-CdS vs. Pt/hex-CdS). A smaller enhancement of 1.6-fold was observed for the same samples with the $S^{2-}/SO_3^{2-}/H_2O$ electron donor system.

As previously noted by Jin et al.[4], the photocatalytic dehydrogenation of aliphatic alcohols can be initiated by reaction with surface bound hydroxyl radicals, which are generated at the surface of CdS. However, based on our previous work[19,20], another possible mechanism for the photocatalytic production of H_2 with visible light is feasible. Hex-CdS, bulk-phase c-CdS, and quantum-sized c-CdS react readily with water as follows:

$$\left[\begin{matrix} S^{2-} \\ Cd^{2+} \end{matrix} > (CdS) \right]_2 + H_2O \xrightleftharpoons{K_H} \begin{matrix} S^{2-} \\ Cd^{2+} \end{matrix} > Cd(II)SH + \begin{matrix} S^{2-} \\ Cd^{2+} \end{matrix} > S(-II)Cd(II)OH \qquad (6.2)$$

The hydrolyzed surface sites, >Cd(II)SH and > CdOH, undergo the following proton transfer reactions:

$$\overset{S^{2-}}{\underset{Cd^{2+}}{}}>CdSH_2^+ \overset{K_{a1}^s}{\rightleftharpoons} \overset{S^{2-}}{\underset{Cd^{2+}}{}}>CdSH + H^+ \quad (6.3)$$

$$\overset{S^{2-}}{\underset{Cd^{2+}}{}}>CdSH \overset{K_{a2}^s}{\rightleftharpoons} \overset{S^{2-}}{\underset{Cd^{2+}}{}}>CdS^- + H^+ \quad (6.4)$$

$$\overset{S^{2-}}{\underset{Cd^{2+}}{}}>CdOH_2^+ \overset{K_{a1.1}^s}{\rightleftharpoons} \overset{S^{2-}}{\underset{Cd^{2+}}{}}>CdOH + H^+ \quad (6.5)$$

$$\overset{S^{2-}}{\underset{Cd^{2+}}{}}>CdOH \overset{K_{a2.1}^s}{\rightleftharpoons} \overset{S^{2-}}{\underset{Cd^{2+}}{}}>CdO^- + H^+ \quad (6.6)$$

Upon equilibration in water, the CdS composites can be photo-excited to produce trapped electrons and holes at the various surface sites. In the case of cadmium sulfide, this leads to photo-reduction of a certain fraction of the available surface sites.

$$\overset{S^{2-}}{\underset{Cd^{2+}}{}}>Cd(+II)S(-II)H \xrightarrow{h\nu} \overset{\bar{e}_{cb}}{\underset{h_{vb}^+}{}} \overset{S^{2-}}{\underset{Cd^{2+}}{}}>Cd(+I)S(-I)H \quad (6.7)$$

$$\overset{S^{2-}}{\underset{Cd^{2+}}{}}>Cd(+I)S(-I)H \xrightarrow{h\nu} \overset{\bar{e}_{cb}}{\underset{h_{vb}^+}{}} \overset{S^{2-}}{\underset{Cd^{2+}}{}}>Cd(0)S(0)H \quad (6.8)$$

Electron transfer to form molecular hydrogen may take place at the reduced surface states as follows:

$$\overset{S^{2-}}{\underset{Cd^{2+}}{}}>Cd(0)S(0)H + H^+ \longleftrightarrow \overset{S^{2-}}{\underset{Cd^{2+}}{}}>Cd(0)S(0)H_2^+ \longrightarrow \overset{S^{2-}}{\underset{Cd^{2+}}{}}>Cd(+II)S(0)^+ + H_2 \quad (6.9)$$

On the other hand, isopropanol, sulfide, and sulfite oxidation are initiated at surface-trapped holes (e.g., $>Cd(+II)S(0)^+$) as follows:

$$\overset{S^{2-}}{\underset{Cd^{2+}}{}}>Cd(+II)S(0)^+ + CH_3CH_2OH \rightleftharpoons \overset{S^{2-}}{\underset{Cd^{2+}}{}}>Cd(+II)S(-I)H^+ + CH_3\dot{C}HOH \quad (6.10)$$

$$\overset{S^{2-}}{\underset{Cd^{2+}}{}}>Cd(+II)S(-I)H^+ + CH_3CH_2OH \rightleftharpoons \overset{S^{2-}}{\underset{Cd^{2+}}{}}>Cd(+II)S(-II)H_2^+ + CH_3\dot{C}HOH \quad (6.11)$$

$$2\,H^{\cdot} \longrightarrow H_2 \quad (6.12)$$

$$2\,CH_3\dot{C}HOH \longrightarrow 2\,CH_3CHO + H_2 \quad (6.13)$$

$$\overset{S^{2-}}{\underset{Cd^{2+}}{}}>Cd(+II)S(-II)H_2^+ \longleftrightarrow \overset{S^{2-}}{\underset{Cd^{2+}}{}}>Cd(+II)S(-II)H + H^+ \quad (6.14)$$

In addition, bandgap excitation and subsequent surface trapping of electrons and holes may take place on cadmium hydroxyl surface sites:

$$\overset{S^{2-}}{\underset{Cd^{2+}}{}}>CdOH + \bar{e}_{cb} \longrightarrow \overset{S^{2-}}{\underset{Cd^{2+}}{}}>CdO^- + H^{\cdot} \quad (6.15)$$

At higher pH, the >CdOH surface site may play an important role in the initial steps of proton reduction (a proton bound to O^{2-}) on the surface of CdS.

$$\overset{S^{2-}}{\underset{Cd^{2+}}{}}>CdOH_2^+ \xrightarrow{2\,\bar{e}_{cb}} \overset{S^{2-}}{\underset{Cd^{2+}}{}}>CdO^- + H_2 \quad (6.16)$$

$$\overset{S^{2-}}{\underset{Cd^{2+}}{}}>CdO^- + 2H^+ \longrightarrow \overset{S^{2-}}{\underset{Cd^{2+}}{}}>CdOH_2^+ \quad (6.17)$$

$$\overset{S^{2-}}{\underset{Cd^{2+}}{}}>CdOH \xrightarrow{h^+_{vb}} \overset{S^{2-}}{\underset{Cd^{2+}}{}}>CdOH^{+\cdot} \xrightarrow{CH_3CH_2OH} \overset{S^{2-}}{\underset{Cd^{2+}}{}}>CdOH_2^+ + CH_3\dot{C}HOH \quad (6.18)$$

Elemental platinum, Pt(0), islands serve as transient reservoirs for trapped electrons effectively increasing the lifetime of the trapped states on both hex-CdS and Q-sized c-CdS.

Similar surface reactions take place in the presence of the mixed HS^-/SO_3^{2-}sulfide electron donor systems[21,22]. Sulfite (SO_3^{2-}) and bisulfide (HS^-) are readily oxidized to SO_4^{2-} and polysulfide ions, S_n^{2-}, such as S_4^{2-} and S_5^{2-}, which impart a yellow color to the aqueous suspension at high pH. However, the polysulfide ions may also act as optical filters and effectively compete for the photoreduction of protons[22]. The formation of the yellow polysulfide ions can be suppressed by reaction with sulfite ions to give HS^- and thiosulfate, $S_2O_3^{2-}$. In addition, excess sulfide in solution stabilizes the CdS surface by eliminating surface defects due to photo-corrosion. A plausible mechanism for this sequence is as follows:

$$\overset{S^{2-}}{\underset{Cd^{2+}}{}}>Cd(+II)S(0)^{+} + HS^{-} \rightleftharpoons \overset{S^{2-}}{\underset{Cd^{2+}}{}}>Cd(+II)S(-I)H^{+} + HS^{\cdot} \quad (6.19)$$

$$2\,HS^{\cdot} \longrightarrow H_2S_2 \quad (6.20)$$

$$H_2S_2 \longleftrightarrow 2\,H^{+} + S_2^{2-} \quad (6.21)$$

$$HS_2^{-} + SO_3^{2-} \longrightarrow S_2O_3^{2-} + HS^{-} \quad (6.22)$$

$$\overset{S^{2-}}{\underset{Cd^{2+}}{}}>Cd(+II)S(0)^{+} + SO_3^{2-} \rightleftharpoons \overset{S^{2-}}{\underset{Cd^{2+}}{}}>Cd(+II)S(-I)H^{+} + SO_3^{-\cdot} \quad (6.23)$$

$$2\,SO_3^{-\cdot} \longrightarrow S_2O_6^{2-} \quad (6.24)$$

$$HS^{\cdot} + SO_3^{-\cdot} \longrightarrow S_2O_3^{2-} + H^{+} \quad (6.25)$$

In a recent study[23], we examined a variety of combinations of c-CdS, TiO_2, and Pt to determine optimal synthesis conditions for hybrid nano-composite catalysts suitable for visible light activation ($\lambda > 420$ nm). We found that the specific preparation procedure and order of reagent addition significantly influenced the observed photocatalytic activity of the ternary hybrid catalysts. In these cases, formation of a potential gradient at the interface between cubic CdS and TiO_2 is necessary in achieving the efficient charge separation and transfer. In addition, the mode of Pt deposition on the c-CdS/TiO_2 hybrid catalysts determined the overall hydrogen production efficiency. For example, photoplatinization of the CdS/TiO_2 hybrid [Pt-(CdS/TiO_2)] proved to be much less efficient than an initial Pt photodeposition on naked TiO_2, which was then followed by the deposition of CdS [CdS/(Pt-TiO_2)]. This result is quite similar that observed in the present study using c-CdS and hex-CdS composites. For example, the CdS/(Pt-TiO_2) had a hydrogen production rate ranging from 6 to 9 $\times$ 10^{-3} mol h^{-1} g^{-1}, which was higher by a factor of 3 to 30 than that of Pt-(CdS/TiO_2). The photocatalytic activity of the ternary

catalysts is sensitive to the location of platinum island deposition and synthesis conditions. In both systems, the sensitivity of the preparation method on the hydrogen production activity needs to be considered during the design and synthesis of hybrid photocatalysts.

In conclusion, we have developed a new hybrid photocatalytic system that is based on a mixed-phase cadmium sulfide matrix composed of quantum-sized, cubic CdS and bulk-phase hexagonal CdS interlinked with elemental platinum. This unusual hybrid composite catalyst is efficient for the photochemical production of molecular hydrogen from water with visible light irradiation, while at the same time it appears to be resistant to photocorrosion.

Acknowledgements

Dr. Luciana A. Silva received fellowship support from CAPES (Coordenação de Aperfeiçoamento de Pessoal de Nível Superior), which is Brazil's Ministry of Education Agency responsible for post-graduate training. The research at Caltech was funded by the Hydrogen Energy R&D Center of the 21st Century Frontier Research and Development Program of the Ministry of Science and Technology of Korea.

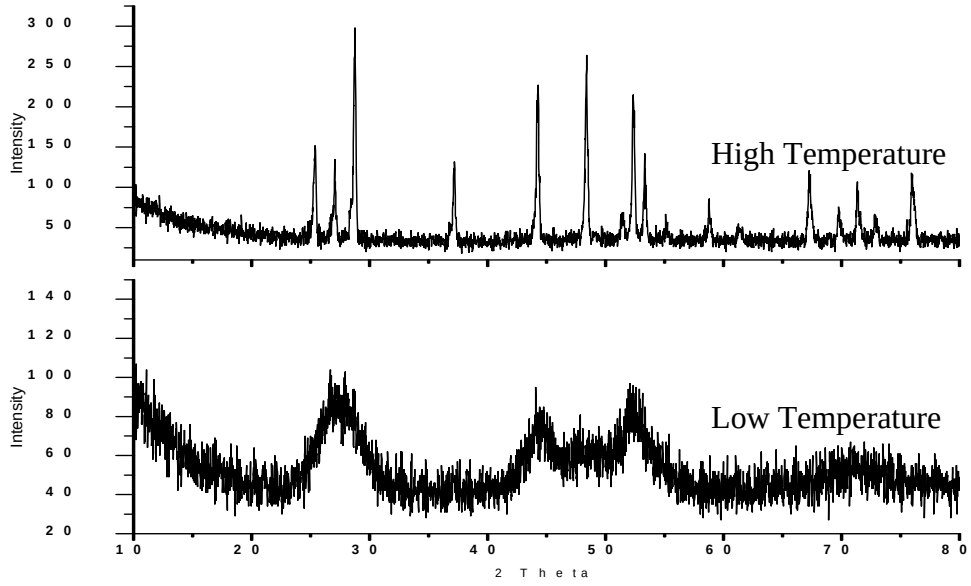

Figure 6.1. X-ray diffraction patterns of comparing the high-temperature, hexagonal phase CdS (hex-CdS) to the thermodynamically favored cubic crystalline bulk-phase CdS (c-CdS)

a)

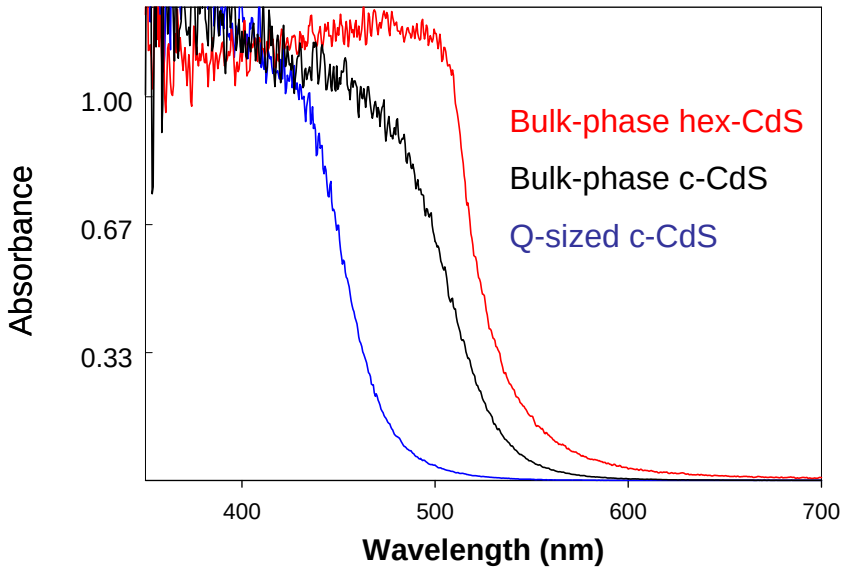

b)

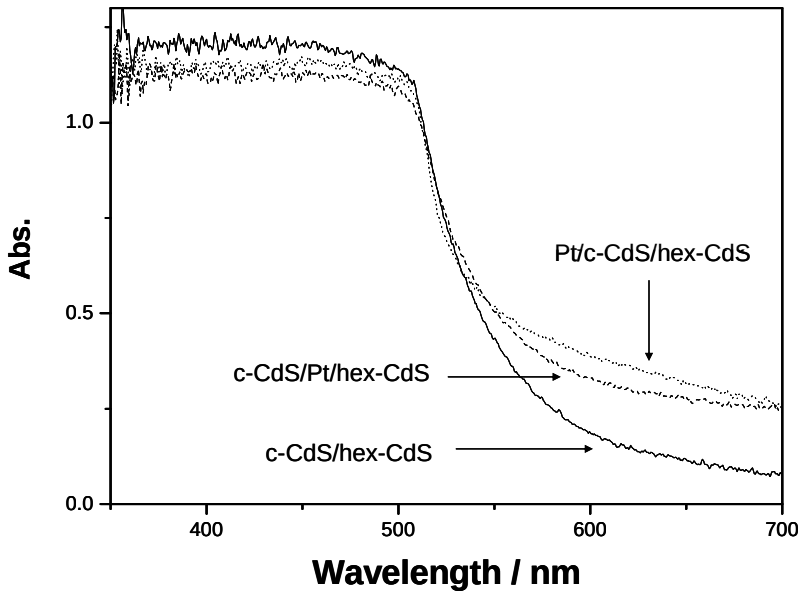

Figure 6.2. Diffuse reflectance spectra of a) the three base CdS materials: quantum-sized c-CdS, yellow crystalline bulk-phase cubic c-CdS, and orange hexagonal hex-CdS; b) the corresponding spectra of the three hybrid nanocomposite catalyts

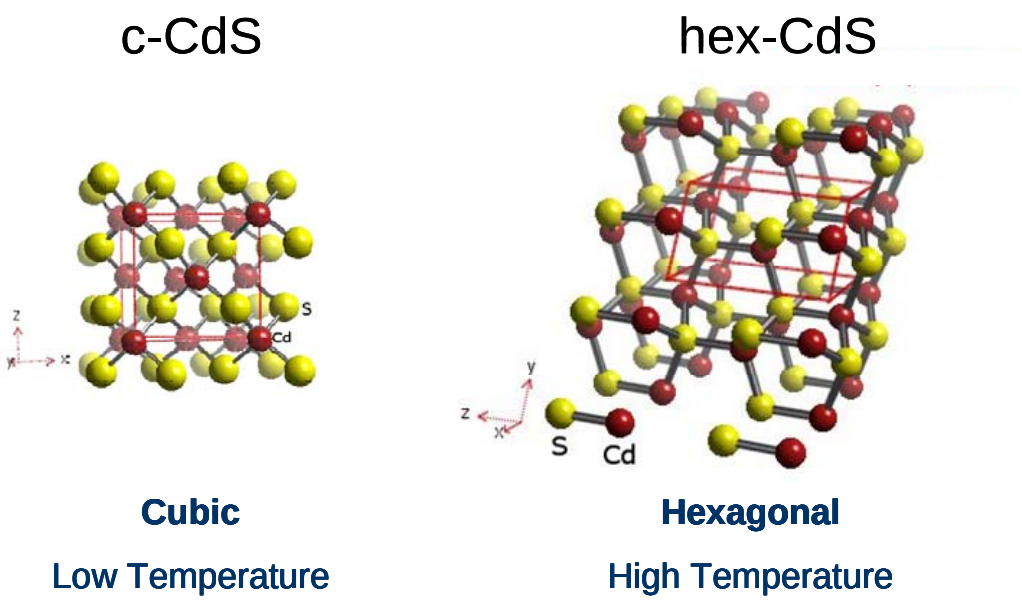

Figure 6.3. The structures of CdS

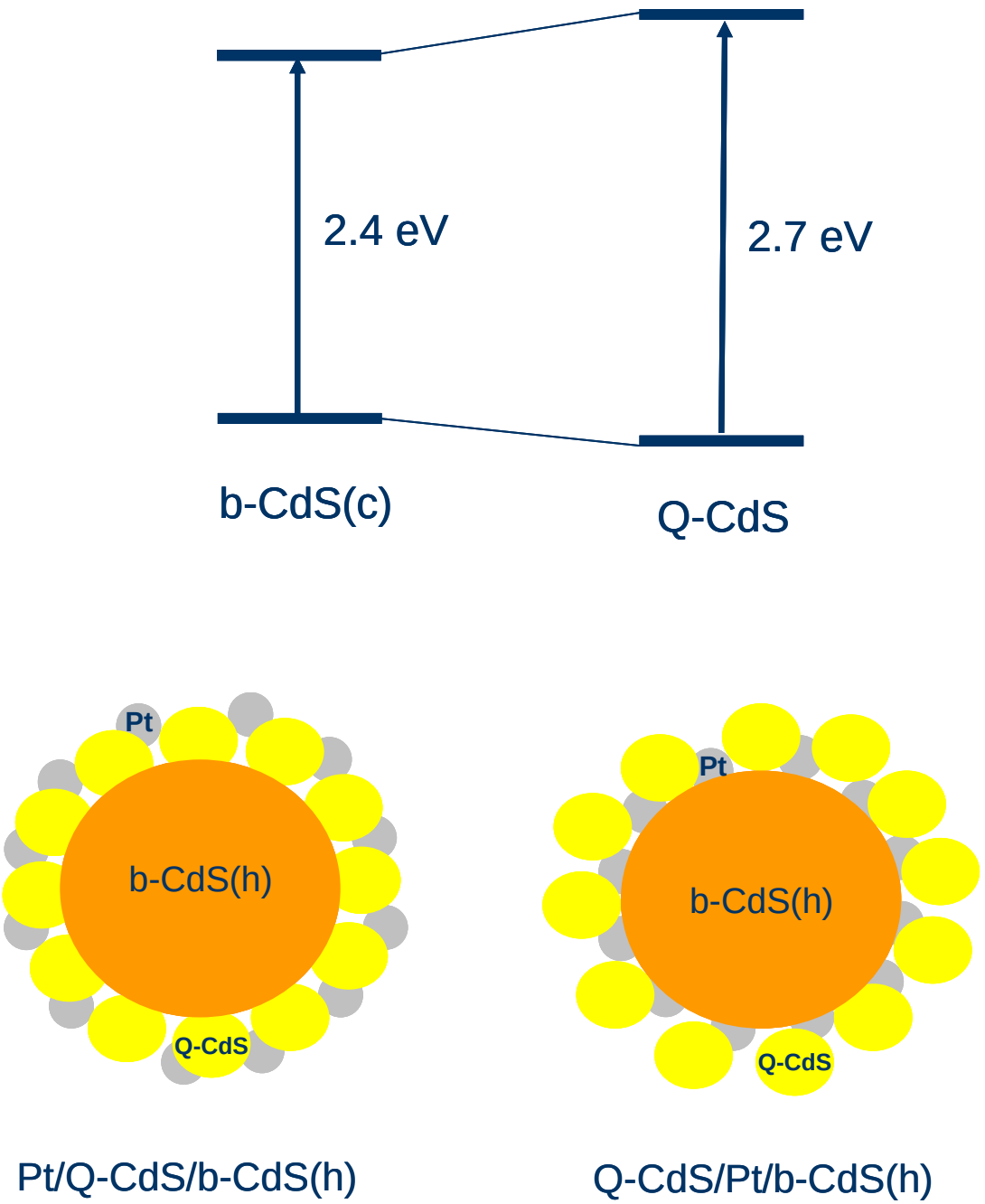

Figure 6.4. The schemes of synthesized nanocomposites

TABLE 6.1. Comparison of the observed rates of hydrogen production over CdS composites from two different aqueous solutions sacrificial electron donors: a) 30% Isopropanol (IPA) in water and b) sulfide/sulfite/hydroxide, 0.1 M Na_2S, 0.02 M Na_2SO_3, and 1.0 M NaOH, with illumination at $\lambda > 400$ nm

Photocatalyst	**$d[H_2]/dt$ (μmol g^{-1} h^{-1})**	
	IPA	S^{2-}/SO_3^{2-}/NaOH
c-CdS/Pt/hex-CdS	153	668
Pt/c-CdS/hex-CdS	1.8	537
c-CdS/hex-CdS	3.5	201
Pt/hex-CdS	45	412
hex-CdS	27	332

References

(1) Matsumura, M.; Ohnishi, H.; Hanafusa, K.; Tsubomura, H. *Bull. Chem. Soc. Jpn.* **1987**, *60*, 2001.

(2) Matsumura, M.; Furukawa, S.; Saho, Y.; Tsubomura, H. *Journal of Physical Chemistry* **1985**, *89*, 1327.

(3) Nosaka, Y.; Yamaguchi, K.; Kuwabara, A.; Miyama, H.; Baba, R.; Fujishima, A. *J. Photochem. Photobiol. A-Chem.* **1992**, *64*, 375.

(4) Jin, Z. S.; Li, Q. L.; Zheng, X. H.; Xi, C. J.; Wang, C. P.; Zhang, H. Q.; Feng, L. B.; Wang, H. Q.; Chen, Z. S.; Jiang, Z. C. *J. Photochem. Photobiol. A-Chem.* **1993**, *71*, 85.

(5) Mills, A.; Green, A. *J. Photochem. Photobiol. A-Chem.* **1991**, *59*, 199.

(6) Janet, C. M.; Viswanath, R. P. *Nanotechnology* **2006**, *17*, 5271.

(7) Jang, J. S.; Li, W.; Oh, S. H.; Lee, J. S. *Chem. Phys. Lett.* **2006**, *425*, 278.

(8) Kormann, C.; Bahnemann, D. W.; Hoffmann, M. R. *Journal of Physical Chemistry* **1988**, *92*, 5196.

(9) Bahnemann, D. W.; Kormann, C.; Hoffmann, M. R. *Journal of Physical Chemistry* **1987**, *91*, 3789.

(10) Hoffmann, M. R.; Martin, S. T.; Choi, W. Y.; Bahnemann, D. W. *Chem. Rev.* **1995**, *95*, 69.

(11) Hoffman, A. J.; Mills, G.; Yee, H.; Hoffmann, M. R. *Journal of Physical Chemistry* **1992**, *96*, 5546.

(12) Martin, S. T.; Morrison, C. L.; Hoffmann, M. R. *Journal of Physical Chemistry* **1994**, *98*, 13695.

(13) Martin, S. T.; Herrmann, H.; Choi, W. Y.; Hoffmann, M. R. *J. Chem. Soc.-Faraday Trans.* **1994**, *90*, 3315.

(14) Martin, S. T.; Herrmann, H.; Hoffmann, M. R. *J. Chem. Soc.-Faraday Trans.* **1994**, *90*, 3323.

(15) Choi, W. Y.; Termin, A.; Hoffmann, M. R. *Journal of Physical Chemistry* **1994**, *98*, 13669.

(16) Hoffman, A. J.; Carraway, E. R.; Hoffmann, M. R. *Environ. Sci. Technol.* **1994**, *28*, 776.

(17) Hoffman, A. J.; Yee, H.; Mills, G.; Hoffmann, M. R. *Journal of Physical Chemistry* **1992**, *96*, 5540.

(18) Lee, J. S.; Choi, W. Y. *J. Phys. Chem. B* **2005**, *109*, 7399.

(19) Ryu, S. Y.; Balcerski, W.; Lee, T. K.; Hoffmann, M. R. *J. Phys. Chem. C* **2007**,

(20) Ryu, S. Y.; Choi, J.; Balcerski, W.; Lee, T. K.; Hoffmann, M. R. *Ind. Eng. Chem. Res.* **2007**, *46*, 7476.

(21) Tsuji, I.; Kudo, A. *J. Photochem. Photobiol. A-Chem.* **2003**, *156*, 249.

(22) Bessekhouad, Y.; Mohammedi, M.; Trari, M. *Sol. Energy Mater. Sol. Cells* **2002**, *73*, 339.